



HAL
open science

Extra-cellular Matrix in cell aggregates is a proxy to mechanically control cell proliferation and motility

Monika Elzbieta Dolega, Sylvain Monnier, Benjamin Brunel, Jean-François Joanny, Pierre Recho, Giovanni Cappello

► To cite this version:

Monika Elzbieta Dolega, Sylvain Monnier, Benjamin Brunel, Jean-François Joanny, Pierre Recho, et al.. Extra-cellular Matrix in cell aggregates is a proxy to mechanically control cell proliferation and motility. 2020. hal-03015345v1

HAL Id: hal-03015345

<https://hal.science/hal-03015345v1>

Preprint submitted on 19 Nov 2020 (v1), last revised 17 Mar 2021 (v2)

HAL is a multi-disciplinary open access archive for the deposit and dissemination of scientific research documents, whether they are published or not. The documents may come from teaching and research institutions in France or abroad, or from public or private research centers.

L'archive ouverte pluridisciplinaire **HAL**, est destinée au dépôt et à la diffusion de documents scientifiques de niveau recherche, publiés ou non, émanant des établissements d'enseignement et de recherche français ou étrangers, des laboratoires publics ou privés.

1 Extra-cellular Matrix in cell 2 aggregates is a proxy to 3 mechanically control cell 4 proliferation and motility

5 **Monika E. Dolega¹, Sylvain Monnier², Benjamin Brunel¹, Jean-François Joanny³,**
6 **Pierre Recho^{1*}, Giovanni Cappello^{1*}**

*For correspondence:

Pierre.Recho@univ-grenoble-alpes.fr (PR); Giovanni.Cappello@univ-grenoble-alpes.fr (GC)

7 ¹ Université Grenoble Alpes, Laboratoire Interdisciplinaire de Physique, CNRS, F-38000
8 Grenoble, France; ² Université de Lyon, Université Claude Bernard Lyon 1, CNRS, Institut
9 Lumière Matière, F-69622, VILLEURBANNE, France; ³ Collège de France, PSL Research
10 University, 11 place Marcelin Berthelot, 75005 Paris, France

11

12 **Abstract** Imposed deformations play an important role in morphogenesis and tissue
13 homeostasis, both in normal and pathological conditions. To perceive mechanical perturbations
14 of different types and magnitudes, tissues need appropriate detectors, with a compliance that
15 matches the perturbation amplitude. By comparing results of selective osmotic compressions of
16 cells within multicellular aggregates with small osmolites and global aggregate compressions
17 with big osmolites, we show that global compressions have a strong impact on the aggregates
18 growth and internal cell motility, while selective compressions of same magnitude have almost
19 no effect. Both compressions alter the volume of individual cells in the same way but, by draining
20 the water out of the extracellular matrix, the global one imposes a residual compressive
21 mechanical stress on the cells while the selective one does not. We conclude that, in aggregates,
22 the extracellular matrix is as a sensor which mechanically regulates cell proliferation and
23 migration in a 3D environment.

24

25 1 Introduction

26 Aside from biochemical signaling, cellular function and fate also depend on the mechanical state
27 of the surrounding extracellular matrix (ECM) (*Humphrey et al., 2014*). The ECM is a non-cellular
28 component of tissues providing a scaffold for cellular adhesion and triggering numerous mechan-
29 otransduction pathways, necessary for morphogenesis and homeostasis (*Vogel, 2018*). An increas-
30 ing number of studies *in vivo* and *in vitro* shows that changing the mechanical properties of the ECM
31 by re-implanting tissues or changing the stiffness of the adherent substrate is sufficient to reverse
32 aging (*Segel et al., 2019*), accelerate developmental processes (*Barriga et al., 2018*) or reverse the
33 pathological state in cancer (*Paszek et al., 2005; Tanner et al., 2012*).

34 The importance of the mechanical context in cancer has for long been highlighted by experiments
35 altering the composition and stiffness of ECM (*Levental et al., 2009*), but more recently it has also
36 been shown that the growth of tumors is modulated by the accumulation of the mechanical pres-
37 sure caused by the hyper-proliferation of cells during tumor expansion in a confined environment
38 (*Fernandez-Sanchez et al., 2010; Nia et al., 2016*). Such physiological growth under pressure has
39 been studied also *in vitro* in the multicellular context. When multicellular aggregates are confined

40 by soft gels (*Helmlinger et al., 1997; Alessandri et al., 2013; Taubenberger et al., 2019*) or submitted
 41 to a gentle osmotic compression (*Montel et al., 2011; Dolega et al., 2017*), their growth is substan-
 42 tially reduced. It has been demonstrated that the cell cytoskeleton is involved in the response to
 43 compression and can trigger the growth impediment through cycle-cell inhibition (*Taubenberger*
 44 *et al., 2019; Delarue et al., 2014*). In addition, cellular volume has been recently proposed to be a
 45 key parameter in the mechanosensitive pathway (*Delarue et al., 2014; Han et al., 2020*). Neverthe-
 46 less, it is not known how such mild global compression is transduced to the individual cells of the
 47 aggregate to alter their proliferation.

48
 49 Here, we introduce the hypothesis that cells
 50 mainly respond to the mechanical stress transmit-
 51 ted by the ECM, when the aggregate is under com-
 52 pression. The hypothesis is motivated by two evi-
 53 dences. First, aggregates are a composite materi-
 54 al made of cells, extracellular matrix and inter-
 55 stitial fluid. The ECM being a soft device 100
 56 to 1000-fold more compressible than the cells, it
 57 absorbs most of the deformation, but still trans-
 58 mits the mechanical stress to the cells. Second,
 59 whereas an osmotic pressure of few kPa strongly
 60 reduces cell proliferation inside multicellular ag-
 61 gregates, an identical pressure has no effect on
 62 individual cells cultured on a Petri dish, in the
 63 absence of ECM.

64 To test the hypothesis that cells respond to the
 65 ECM deformation, we introduce an experimental
 66 method that uncouples the cell volume change
 67 from the mechanical stress transmitted to the
 68 cells through the ECM. We apply this method
 69 for both multicellular aggregates and individual
 70 cells embedded in a gelified ECM. In parallel, we
 71 present a theoretical framework to estimate both
 72 the displacement and the stress at the ECM/cell
 73 interface in response of an osmotic compression,
 74 and verify experimentally its qualitative predic-
 75 tion. At longer timescale, we probe the effect of
 76 the ECM compression on the cellular response, in
 77 terms of proliferation and motility. Our results
 78 show that, even in the absence of cell deformation, the ECM deformation alone is an important
 79 factor determining these properties.

80 2 Results

81 2.1 Selective-compression method

82 We developed a simple method to either selectively compress cells embedded in ECM or the whole
 83 complex composed of ECM and cells. This method is based on the use of osmolytes of different
 84 sizes. When large enough, the osmolytes do not infiltrate the ECM and thus compress the whole
 85 complex by dehydrating the ECM, which in turn mechanically compresses the cells (*Monnier et al.,*
 86 *2015*). When smaller than the exclusion size of the ECM, the osmolytes percolate through the ECM
 87 meshwork and selectively compress the cells which can then pull on the ECM (see schema in fig-
 88 ure 1). We validate our approach by compressing ECM, cells and multicellular spheroids (MCS)

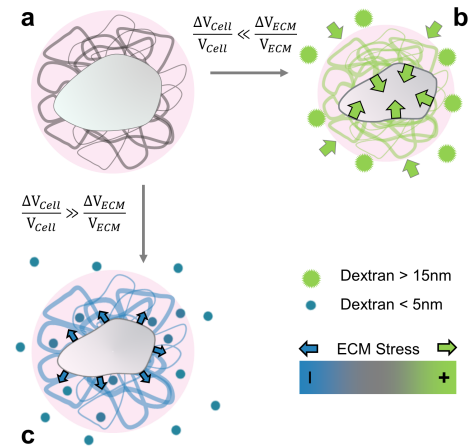


Figure 1. Selective compression method. **(a)** Schematic view of a cell (gray) embedded in extracellular matrix (filaments), permeated by interstitial fluid (light pink). **(b)** Big osmolytes (green) do not penetrate through the ECM and induce a global compression. Being much more compressible than the cells, the extracellular matrix absorbs most of the deformation and exert a positive stress on the cell. **(c)** Small osmolytes (blue) enter the ECM without exerting any osmotic pressure on it. Conversely, they compress the cell which, in turn, exerts a tension on the ECM.

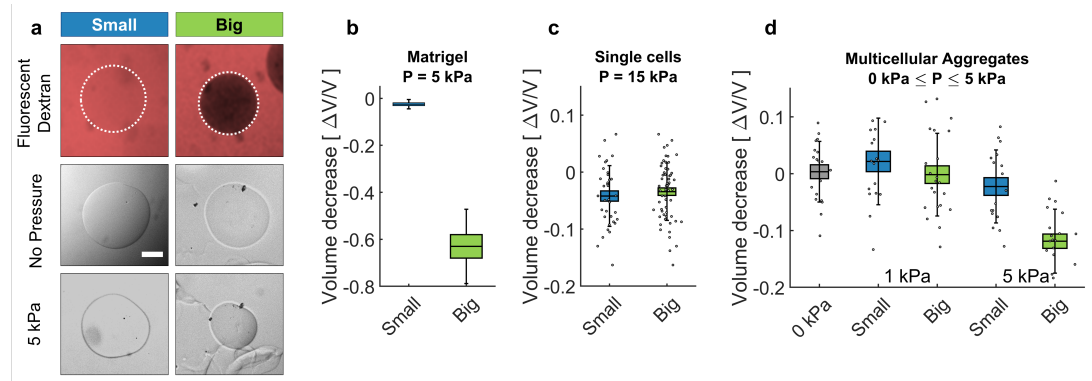


Figure 2. Cell and Matrigel Compression. (a) Fluorescently labeled dextran molecules only permeate the beads (top-left panel) only if their gyration radius is smaller than 5 nm. Otherwise (top-right panel) they are larger of the exclusion size of the matrigel network and are excluded from the bead. Compression of MG beads, occasioned by dextran molecule of two different sizes (Small: 70 kDa; Big: 500 kDa). Phase contrast images taken before and after the addition of pressure. (b) Beads lose $63 \pm 5\%$ of their initial volume when compressed using big dextran, and approximately 2.5 % with small Dextran. $N=10$. (c) Compression of individual cells using dextran of different sizes, corrected for a final pressure of about 15 kPa. At 5 kPa the compressibility of individual cells is not measurable. Cell compressibility is thus negligible in comparison to that of Matrigel. (d) MCS relative compression under a pressure of 1 kPa and 5 kPa, exerted using small (blue) and big (green) dextran molecules. (box : \pm SEOM; error bars: \pm SD • : single realizations).

89 using osmolytes with gyration radii R_g respectively larger and smaller that the ECM pore sizes (figure 2). As osmolytes, we use dextran molecules ranging from 10 to 2000 kDa. As a proxy of ECM, 90 we use Matrigel (MG), a commercially available matrix secreted by cancer cells (Kleinman and Martin, 2005). To visualize the effect of compression on the ECM, we prepared microbeads composed 91 of matrigel, with a diameter of $100 \mu\text{m}$ (fig. 2a). To determine the exclusion size of matrigel, we use 92 fluorescent dextran molecules of different gyration radii. As shown in figure 2a (top panel), fluorescent dextran molecules with a gyration radius below 5 nm (MW < 70 kDa, hereafter called "Small"; 93 (Granath, 1958)) equally color the MG beads and the surrounding solution (left). Conversely, dextran molecules larger than 15 nm (MW > 500 kDa, "Big") do not penetrate inside the MG beads, 94 which appear darker than the surroundings (right). By following the evolution of the bead diameter (before and after 45 minutes) under a 5 kPa compression, we confirmed that small dextran 95 molecules do not compress significantly the matrigel beads (figure 2a, middle and bottom panels). 96 The small amount of compression, which we neglect, can be addressed by thermodynamic theories involving an interaction between the matrix and the permeating polymer (Brochard, 1981; 97 Bastide et al., 1981). Conversely, big dextran molecules occasion a large compression of up to 98 $63 \pm 5\%$ of the initial volume (quantification in figure 2b).

99 Analogous experiments are performed using individual cells and multicellular spheroids. Interestingly, the volume loss of individual cells is not measurable up to 10 kPa, and becomes appreciable at 15 kPa, with a relative compression $\Delta V_c/V_c = 5 \pm 5\%$ (figure 2c). This compression 100 indicates that CT26 cells have a bulk modulus $K_c = 450 \pm 100 \text{ kPa}$. In contrast to single cells, MCS 101 are much more compressible, as they lose up to 15% of their volume under a pressure of 5 kPa (figure 2d). Furthermore, these measurements indicate that MCS have a typical bulk modulus of $K_s \approx$ 102 30 kPa , 15-folds smaller than that of individual cells. In contrast, small dextran molecules have no 103 measurable effect on the volume of MCS, for moderate pressures (up to 10 kPa). However, larger 104 pressures with these small osmolites can lead to a cell compression within the MCS associated with a swelling of the interstitial space as we show in Section 2.3.

105 These results confirm the ability of our method to discriminate between the effects occasioned 106 by the compression of the whole MCS, and that due to the specific compression of the cells within 107 the aggregate. 108 109 110 111 112 113 114 115 116 117

118 2.2 Theoretical understanding of the selective compression of composite aggregates

119
120 Our aim is to compute the displacement of the cell boundary as well as the stress applied on the cell
121 upon the osmotic compression in both conditions. For simplicity, we consider the case of a single
122 cell nested in a large -compared to the cell size- ball of ECM and subjected to an additional osmotic
123 pressure Π_d (i.e. added to the existing pressure in the culture medium) obtained by supplementing
124 the culture medium with either small or big dextran. We assume that the small dextran can freely
125 permeate in the ECM meshwork while the big one is excluded. Our model, detailed in Section A.5,
126 couples a classical active pump and leak model (*Hoppensteadt and Peskin, 2012*) for the cell volume
127 regulation through ion pumping and the cytoskeleton and the ECM poro-elastic mechanics.

128 We show in Section A.5 that, for realistic estimates of the model parameters, both compressions
129 with small and big dextran lead to the same cell volume loss which does not involve the mechanical
130 properties of the ECM but only the cell volume regulation system:

$$\frac{\Delta V_c}{V_c} = \frac{\Pi_d}{(1 - \beta)\Pi_e}, \quad (1)$$

131 where Π_e is the osmotic pressure of ions in the culture medium and $\beta \simeq 0.1$ is a non-dimensional
132 parameter representing the active pumping of ions (see Appendix A.4). For relatively low pressures
133 ($\Pi_d \ll \Pi_e \simeq 500$ kPa), the relative change of volume $\Delta V_c/V_c$ is negligible. However, the mechanical
134 stress applied by the ECM to the cell is qualitatively and quantitatively different in the two situ-
135 ations. For big dextran, this stress is compressive as the dominating effect of the dextran is to
136 compress the ECM which in turn compresses the cell by the same amount. Within some realistic
137 approximations the amount of this compressive stress (the traction force applied by the matrix on
138 the cell) can be approximated as the applied osmotic pressure:

$$T_{\text{big}} = -\Pi_d < 0, \quad (2)$$

139 In sharp contrast with the previous situation, for small dextran, the stress applied by the ECM on
140 the cell is tensile because the dominating effect is that small dextran does not compress the ECM
141 but acts on the cell which compression is balanced by a tensile force in the ECM. This tension is
142 given by

$$T_{\text{small}} = \frac{G \Pi_d}{3(1 - \beta)\Pi_e} > 0, \quad (3)$$

143 where G is the ECM shear modulus. Again, for a moderate osmotic shock of $\Pi_d \simeq 5$ kPa, the
144 dextran concentration is much smaller than the characteristic ions concentration of the external
145 medium and $T_{\text{small}} \leq 20\text{Pa} \ll |T_{\text{big}}|$. Therefore the presence of ECM makes the cell mechanically
146 sensitive to a moderate osmotic compression by big dextran molecules while it is not for small
147 dextran molecules. In both cases the cell volume is affected in the same negligible way but the
148 mechanical stresses applied to the cell are completely different. If the osmotic compression is
149 larger, compression with small or big dextran can induce a measurable effect on the cell volume.
150 However, the mechanical stress applied by the ECM to the cell is different in both situations: tensile
151 for the small dextran and compressive for the big ones.

152 2.3 Selective compression of ECM in multicellular spheroids.

153 To test our theoretical predictions, we follow the evolution of the interstitial space inside MCS sub-
154 mitted to osmotic compression, occasioned either by small or big dextran. To improve the optical
155 performance and to measure changes in the extracellular space after compression by small and
156 big dextran, we inject the spheroids (4-5 days old) into a 2D confiner microsystem (figure 3a). MCS
157 are confined in the microsystem for two to five hours to relax, the medium being supplemented
158 with a fluorescent tracer to label the intercellular space. The interstitial fluorescence is measured
159 using two-photon microscopy (figure 3b). The images of the confined multicellular aggregates are
160 segmented with a thresholding procedure, and then the signal exceeding the threshold value is

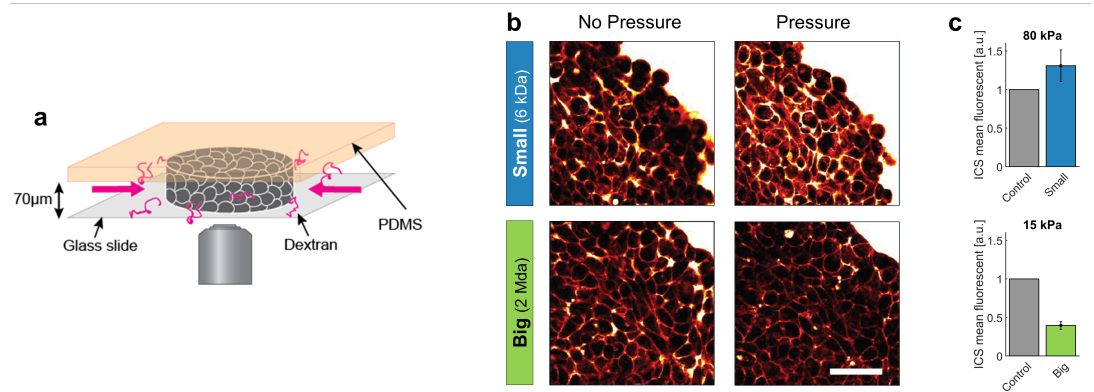


Figure 3. Effect of small versus big dextran on tissue intercellular space. (a) Scheme of the 2D confiner micro-device. The tissue is confined between the glass coverslip and the PDMS and does not move during medium exchange. (b) 2-photon images of the tissue before and after (20min) osmotic shocks for dextran chains of 6kDa (small) and 2MDa (big), for a given mass concentration of 100g/L. Images were taken in the equatorial plane of the tissue, meaning 35µm above the glass slide. (c) Mean fluorescence of the intercellular space averaged over the whole aggregate shown in panel B. Scale Bar: 50µm

161 integrated over the whole aggregate to quantify the total fluorescence of the interstitial space (figure 3c). Due to optical limitations, we emphasize the effect by increasing the applied osmotic
 162 pressure to 80 kPa for small dextran and to 15 kPa for the big ones.

164 In accordance with the theoretical predictions, depending on the dextran size, we obtain two
 165 opposite behaviors. Small dextran molecules induce an increase of ~ 50% in the fluorescence in-
 166 tensity, measured in the interstitial space. As the total volume of the aggregate does not change
 167 significantly (figure 2d), the swelling phenomenon is related to a cell deflation compensated by the
 168 ECM swelling. In contrast, for Big dextran we measure a loss of half the fluorescence, meaning
 169 that a large amount of interstitial liquid has left the aggregate. With big osmolytes, the extracel-
 170 lular matrix is thus compressed as predicted by eq.(2), while the loss of cell volume is negligible
 171 compared to the latter effect. These results confirm the theoretical prediction that big and small
 172 dextran have an opposite effect on the matrix. The first puts the ECM under compression, while
 173 the latter puts the ECM under tension.

174 2.4 ECM compression controls cell proliferation and motility

175 To understand the role of ECM on the cell fate at longer timescale, we assess the proliferation and
 176 the motility for MCS cultured in the presence of small and big dextran. Figure 4a represents the
 177 equatorial cryosections of spheroids in the three mechanical states. Proliferating cells are labeled
 178 using antibodies against KI67. Whereas cells in control MCS (0 kPa) present a rather uniform pro-
 179 liferation pattern, a global compression of MCS (big Dextran) stops cell division in the core and
 180 alters the overall MCS growth, as previously reported (Helmlinger et al., 1997; Alessandri et al.,
 181 2013; Montel et al., 2011). To quantify the change of cell division rate, we monitor the volumetric
 182 growth of the spheroid for three conditions (control, small dextra, big dextran) and for several days
 183 (figure 4b). In the three cases, the spheroids initially grow exponentially (continuous lines). How-
 184 ever, the cell division time almost doubles under compression and increases from 36 ± 1 h (gray
 185 circles and blue squares) to 68 ± 4 h (5 kPa, green triangles). Because experiments with MCS are
 186 typically performed in solution, where metastatic behavior is not possible, we evaluate the cell
 187 motility within the aggregate, using the Dynamic Light Scattering technique introduced by Brunel
 188 et al. (2020). The mean migration velocity of cells decreases monotonously with the pressure and
 189 is reduced by 50% at 5 kPa, as compared to the unstressed case (figure 4c). Strikingly, both prolifer-
 190 ation and motility remain almost unaltered when the MCS are exposed to an equivalent pressure
 191 (5 kPa) applied with small dextran to selectively compress the cells while leaving the native ECM

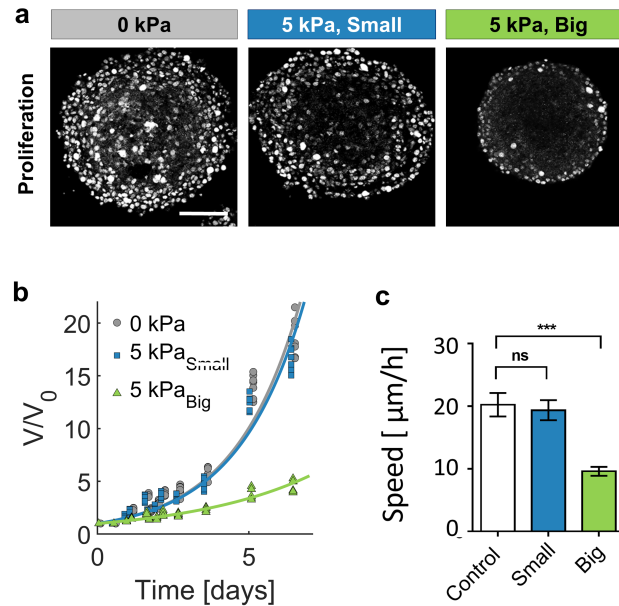


Figure 4. Growth of spheroids under pressure. (a) Proliferating cells inside MCS revealed by immunostaining of KI67 with no pressure, under overall compression of 5 kPa (big dextran) and under selective compression of the cells (small dextran). Scale bar: 100 μm **(b)** Volume increase of spheroids over several days, in the three reference conditions. **(d)** Cell migration speed (see SI) within MCS also significantly depends on ECM compression. $N=5$ independent experiments per condition. Error bars represent \pm SEM. Experiments are repeated at least on three independent samples.

192 unstrained (small Dextran, blue).

193 Since the interstitial space is dehydrated under osmotic compression, it is possible that the
 194 cells get in contact with each other, occasioning contact inhibition of proliferation and locomotion.
 195 However, it is also possible that cells read and react to the stress accumulated in the ECM. To
 196 discriminate between these two hypothesis, we embed individual cells in a MG matrix and then
 197 compress the whole system with a 5 kPa osmotic pressure using either small or big dextran. After
 198 a few days, we observe two clearly different phenotypes. Cells that have grown without pressure
 199 are sparse in the MG, as well as cells that have proliferated in the presence of small dextran (fig-
 200 ure 5a, left panel). Conversely, when cells are cultured in the presence of big dextran, they prolifer-
 201 ate locally (figure 5a, right panel). Therefore, MG compression appears to inhibit cell motility and
 202 to promote the formation of mini-spheroids, which suggests that ECM compression has a direct
 203 effect on the cell-ECM biochemical signaling. The different cell morphology is particularly clear in
 204 the organization of the actin cytoskeleton. Cytoplasmic actin labeling reveals the presence of nu-
 205 merous protrusions, associated with high cell anisotropy in cells cultured in a relaxed MG matrix
 206 (figure 5b, left and middle panels), whereas cells appear smooth and form round structures, when
 207 the MG is compressed (figure 5b, right panel).

208 Different morphology also correlates with different motility. Cells embedded in a compressed
 209 MG are nearly immobile, while they migrate through relaxed MG with a velocity comparable to that
 210 measured on flat surfaces. The result is summarised in figure 5c, where we report ≈ 40 trajec-
 211 tories per condition. To highlight differences and similarities between the three compression states,
 212 the starting points of all trajectories are translated to the origin and, whereas isotropic, they are
 213 compressed in three quadrants. Quantification is reported in figure 5d. From this experiment we
 214 conclude that whereas no appreciable differences are observable between the case where the MG
 215 is relaxed and the control, the cell motility dramatically drops under MG compression.

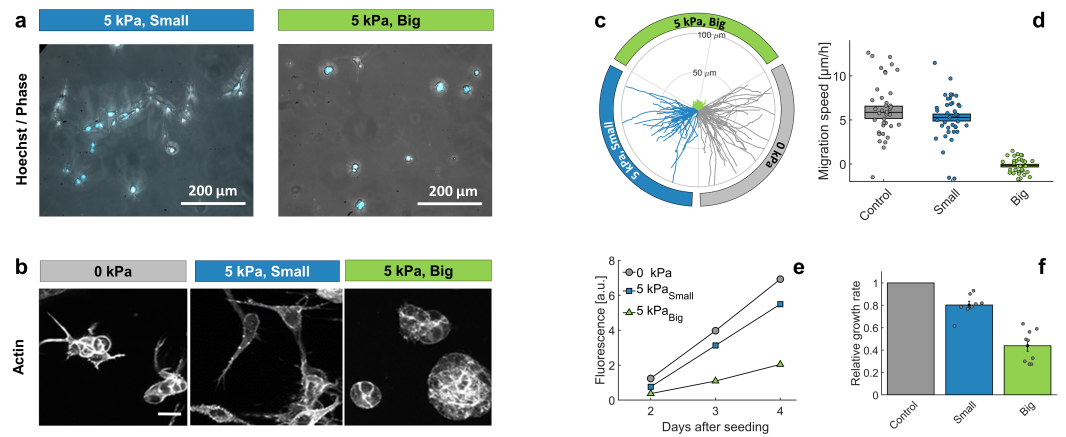


Figure 5. Individual cells in Matrigel. (a) Hoechst-labelled cell nuclei superimposed to phase image (maximum intensity z-projection). Images are taken after 2 days of proliferation in MG, either with small (left panel) or big (right panel) dextran molecules. Maximal projection from epifluorescence stacks. (b) Cell morphology and anisotropy revealed by labelling of cytoplasmic actin. Maximal projection of 50 μm confocal Z-stack. In relaxed MG, the cells appear more elongated and with long protrusions. (c) Cell motility in MG under different compression states. Starting points of trajectories are translated to the origin, to highlight the typical distance over which cells move in the three compressive states. (d) Quantification of in-plane velocity extracted from mean square displacements, under different compression conditions. With no pressure or with small dextran (5 kPa), the average velocities are respectively $5.8 \pm 0.8 \mu\text{m/h}$ and $5.2 \pm 0.5 \mu\text{m/h}$. Under 5 kPa exerted by big dextran, the cells are immobile ($v = 0.5 \pm 0.4 \mu\text{m}$), where the error is due to tracking uncertainties. Boxes represent the average speed \pm SEOM. (e) Temporal evolution of nuclear fluorescence integrated over the whole sample. No pressure (\circ), 5 kPa with small dextran (\square) and 5 kPa with big dextran (\triangle). (f) Cell proliferation rate in the three conditions. $n = 15$, from 8 independent experiments.

216 To quantify the effect of ECM compression on proliferation, we prepare several samples with
 217 the same number of cells embedded in the MG and follow the evolution of the overall fluorescence
 218 (hoechst staining) in time. Figure 5e shows the typical time evolution of the Hoechst signal in the
 219 three conditions: proliferation rate drops considerably when the MG is compressed (Big Dextran,
 220 \triangle), compared to the case without pressure (\circ), but also compared to the case where the pressure is
 221 selectively exerted on the cells with no MG compression (Small Dextran, \square). Figure 5f quantifies the
 222 mean growth rate, measured on at least 15 samples for each condition, collected on 8 independent
 223 experiments (different days and cell passages). Again, these experiments underline the impact of
 224 the ECM compressive stress on cell behavior.

225 3 Discussion and Conclusion

226 Large osmotic and mechanical pressures (≈ 100 kPa), can cause a decrease in cell volume and con-
 227 sequently a deformation of the cell nucleus (Zhou *et al.*, 2009; Kim *et al.*, 2015) which may ultimately
 228 feedback on the cell proliferation. It has been proposed lately that the volume of cells or nucleus
 229 can be a key parameter governing crucial processes such as proliferation, invasion and differen-
 230 tiation Guo *et al.* (2017); Han *et al.* (2020). However the weak osmotic pressures (~ 1 kPa) that
 231 we apply have no measurable effect on cell volume. In addition, it is well-known from a biologi-
 232 cal standpoint that such small volume perturbations are buffered by active regulatory processes
 233 in the cell (Hoffmann *et al.*, 2009). Yet, in MCS both proliferation and cell motility decrease when
 234 the aggregate undergoes a weak osmotic compression. Altogether, our results show that, for such
 235 weak compressions, the extracellular matrix (ECM) located in between the cells is directly impacted
 236 but not the cell volume. Moreover, the presence of ECM could explain the reported evidences that
 237 mechanical and osmotic pressures of same magnitudes affect the growth of MCS in the same way
 238 (Helmlinger *et al.*, 1997; Alessandri *et al.*, 2013; Montel *et al.*, 2011) for osmotic pressures applied

239 via macromolecules large enough not to penetrate the extracellular matrix. Indeed, the osmotic
 240 pressure is transduced into a mechanical one applied on the cells through the ECM drainage. As
 241 the ECM has a bulk modulus $K_{ECM} \simeq 1$ kPa, it can serve as sensor to measure, at the cell level, a glob-
 242 ally applied pressure in the kPa range. Of note, stress relaxation in the ECM could occur through
 243 cleavage and remodeling of its components and such active processes should be quantified in the
 244 future.

245 Several mechanisms may explain how the dehydration of the extracellular matrix can result in
 246 an inhibition of proliferation and motility. First, the reduction of the interstitial space promotes
 247 interactions between neighbouring cells, which may activate contact inhibition signals of both pro-
 248 liferation and locomotion (*Roycroft and Mayor, 2016*). Second, the ECM porosity decreases within
 249 a compressed MCS, such that its effective permeability to oxygen, nutrients, growth factors and
 250 cytokines is reduced and might activate inhibition signals without cell-cell contact. However, both
 251 options appear incompatible with experiments of individual cells seeded in MG (Figure 5). Indeed,
 252 in these experiments, cells are isolated until the first division events. Then, when they form aggre-
 253 gates these have a very large surface-to-volume ratio compared to MCS, indicating that collective
 254 effects mediated by cell-cell contacts are unlikely to explain why cells decrease their proliferation.
 255 Additionally, in MCS, a key factor limiting the availability for cells of oxygen and nutrients present
 256 in the culture medium is the tortuosity of the interstitial space (*Bläßle et al., 2018*). This constraint
 257 is simply absent in experiments with single cells embedded in MG, such that the cell proliferation
 258 inhibition is most probably not related to hypoxia and starvation.

259 The present work therefore points at a direct mechanosensitive response of cells to the de-
 260 formation accumulated in the ECM. The microscopic structure of the ECM is modified under com-
 261 pression (e.g. density increase, decrease of distances between cross-links and buckling of collagen
 262 fibers), with consequences on the ECM rheology. Compression is clearly accompanied by an in-
 263 crease in bulk modulus and, due to the fibrillar structure, to a non-trivial and non-linear evolution
 264 of the ECM stiffness (*Sopher et al., 2018; Kurniawan et al., 2016*). For example, the rheological prop-
 265 erties of synthetic ECM have been shown to affect growth of aggregates and single cells through
 266 the regulation of stretched-activated channels (*Nam et al., 2019*). As integrin-dependent signals
 267 and focal adhesion assembly are regulated by the stress and strain between the cell and the ECM,
 268 the osmotic compression may steer the fate of eukaryotic cell in terms of morphology, migration
 269 and differentiation (*Pelham and Wang, 1997; Choquet et al., 1997; Sunyer et al., 2016; Isenberg
 270 et al., 2009; Butcher et al., 2009; Engler et al., 2006; Staunton et al., 2019; Panzetta et al., 2019*).
 271 This aspect is also relevant from an oncological point of view. Indeed the ECM is strongly modified
 272 in tumour tissues and the solid stress within tumors can reach several kPa, which is in accordance
 273 with the pressure applied here (*Nia et al., 2016*). For example, there is a decrease in the ratio col-
 274 lagen/hyaluronan (*Voutouri et al., 2016*). The latter, more hydrophilic than the first one, tends to
 275 swell and stiffen the ECM. Whether a corrupted matrix is a contributing cause or the consequence
 276 of the neoplasia remains an open question, but the correlation between matrix mechanics and un-
 277 controlled proliferation is more and more widely accepted (*Bissell et al., 2002; Lelièvre and Bissell,
 278 2006; Broders-Bondon et al., 2018*).

279 In future experiments, by varying the ECM density and consequently its rheology in a controlled
 280 manner, it will be crucial to identify whether the ECM compression and the associated changes in
 281 stiffness plays a dominant role, or if - as we suggest - the mechanical stress applied on the cell
 282 through the ECM is the key ingredient directly triggering the cell biological adaptation in term of
 283 proliferation and motility.

284 4 Acknowledgements

285 We warmly thank J. Prost and F. Jülicher for drawing our attention to the potential impact of the
 286 poroelasticity in MCS, A. Dawid and J. Revilloud for the valuable suggestion to set the proliferation
 287 assay in MG, and C. Verdier for the valuable exchanges about the evolution of the ECM rheology

288 under stress. This work was supported by the Agence Nationale pour la Recherche (Grant ANR-13-
 289 BSV5-0008-01), by the Institut National de la Santé et de la Recherche Médicale (Grant PC201407),
 290 by the Centre National de la Recherche Scientifique (Grant MechanoBio 2018), by the Comité de
 291 Haute-Savoie de la Ligue contre le Cancer, and by a CNRS Momentum grant (P.R.)

292 **5 Methods and Materials**

293 **5.1 Cell culture, MCSs formation, and growth under mechanical stress**

294 CT26 (mouse colon adenocarcinoma cells, ATCC CRL-2638; American Type Culture Collection are
 295 cultured under 37°C, 5% CO₂ in DMEM supplemented with 10% calf serum and 1% antibiotic / an-
 296 timycotic (culture medium). Spheroid are prepared on agarose cushion in 96 well plates at the con-
 297 centration of 500 cell/well and centrifuged initially for 5 minutes at 800rpm to accelerate aggrega-
 298 tion. After 2 days, Dextran (molecular mass 1, 10, 40, 70, 100, 200, 500 and 2000 kDa; Sigma-Aldrich,
 299 St. Louis, MO) is added to the culture medium to exert mechanical stress, as previously described
 300 (*Monnier et al., 2015*). To follow spheroid growth over the time, phase contrast images are taken
 301 daily. Spheroid are kept under constant pressure over observation period. Images are analysed
 302 manually using Imagej. Each experiment was repeated 3 times, with 32 individual spheroids per
 303 condition.

304 **5.2 Fabrication of Matrigel beads**

305 Matrigel beads are prepared using vortex method (*Dolega et al., 2017*). Oil phase of HFE-7500/PFPE-
 306 PEG (1.5% w/v) is cooled down to 4°C. For 400 μL of oil, 100 μL of Matrigel is added. Solution is vor-
 307 texed at full speed for 20 seconds and subsequently kept at 37°C for 20 minutes for polymerization.
 308 Beads are eventually transferred to PBS phase by washing out the surfactant phase.

309 **5.3 Fluorescence eXclusion method (single cell volume measurements)**

310 Cell volume is obtained using Fluorescence Exclusion microscopy (*Cadart et al., 2017; Zlotek-Zlotkiewicz*
 311 *et al., 2015*). Briefly, cells are incubated in PDMS chips, with medium supplemented with a fluores-
 312 cent dye that does not enter the cells. Cells thus exclude fluorescence, and one extracts cellular
 313 volume by integrating the fluorescence intensity over the whole cell. Chips for volume measure-
 314 ments of single cells are made by pouring a mixture (1:10) of PMDS elastomer and curing agent
 315 (Sylgard 184) onto a brass master and cured at 80°C for at least of 2 hours. Inlet and outlets were
 316 punched with a 3mm biopsy puncher. Chips are prepared few days before, bounded with oxy-
 317 gen plasma for 30s, warmed up at 80°C for 3 minutes then incubated with Poly-L-lysine (sigma) for
 318 30min to 1hrs, washed with PBS, then washed with dH₂O, dried and stored sealed with a paraffin
 319 film. The chambers are washed with PBS before cell injection. Imaging starts within 10 minutes af-
 320 ter cell injection in order to prevent adhesion and thus cells response to the shear stress generated
 321 by the medium exchange. Acquisition is performed at 37°C in CO₂ independent medium (Life Tech-
 322 nologies) supplemented with 1g/L FITC dextran (10kDa, from Sigma Aldrich) on an epifluorescence
 323 microscope (Leica DMI8) with a 10x objective (NA. 0.3 from LEICA).

324 **5.4 2D Confiner**

325 The 2D confiner is microsystem conceived to image three-dimensional multicellular aggregates
 326 with a two-photon microscope (see figure 3a). Spheroids (4-5 days old) are injected in the device
 327 using a pressure controller (Fluigent, MFCS) and are partially flattened between two parallel sur-
 328 faces, perpendicular to the optical axis of the microscope. Medium perfusion and exchanges is
 329 performed manually using large inlets (>1 mm) during two-photon acquisition. Acquisitions are
 330 performed at 37°C on a Nikon C1 two-photon microscope coupled with a femtosecond laser at
 331 780nm with a 40x water-immersion (NA. 1.10) objective (Nikon). Chip is made by pouring PDMS
 332 elastomere and curing agent (1:10) the mold and cured for at least 2 hours. The chips are bounded
 333 to glass coverslips with 30s oxygen plasma, immediately after bounding, a solution of PLL-g-PEG

334 at 1g/L (to check) is injected and incubated for 30 minutes in humid atmosphere to prevent cell
335 surface adhesion during the experiment. The chips are washed with dH₂O, dried and sealed with a
336 paraffin film.

337 **5.5 Cell culture in Matrigel**

338 Experiments are conceived to start the culture from individual cells embedded in Matrigel. At day
339 1, the cells are resuspended, then dispersed in a solution containing matrigel at the final concentra-
340 tion of 4.5 g/l. The cells are diluted to 10,000-50,000 cells/ml, a concentration at which the average
341 distance between neighboring cells is about 250-400 μ m. We therefore consider them as isolated
342 entities. The MG/cell ensemble is gelified in 200 μ l wells, at 37°C, for 30 minutes. To avoid cell sed-
343 imentation, we gently flip the sample over, every two minutes. The samples are then redeposited
344 in the incubator under three pressure conditions: no pressure and 5 kPa exerted both by small
345 and big dextran.

346 **5.6 Cells Migration in Matrigel**

347 To quantify cell migration in Matrigel, individual cells are observed by phase contrast microscopy. Z-
348 stacks are collected every 20 minutes and for several days, with slices spaced by 50 μ m. Then the full
349 stack is projected to one single layer (maximum intensity projection). Cells are tracked manually in
350 the 2D plane, using the ImageJ MTrackJ plugin (<https://image.science.org/meijering/software/mtrackj/>)

351 **5.7 Cryosectioning and Immunostaining**

352 Spheroids are fixed with 5% formalin (Sigma Aldrich, HT501128) in PBS for 30 min and washed once
353 with PBS. For cryopreservation spheroids are exposed to sucrose at 10% (w/v) for 1 hour, 20% (w/v)
354 for 1 hour and 30% (w/v) overnight at 4°C. Subsequently spheroids are transferred to a plastic reser-
355 voir and covered with Tisse TEK OCT (Sakura) in an isopropanol/dry ice bath. Solidified samples are
356 brought to the cryotome (Leica CM3000) and sectioned into 15 μ m slices. Cut layers are deposited
357 onto poly-L-lysine coated glass slides (Sigma) and the region of interest is delineated with DAKO
358 pen. Samples are stored at -20°C prior immunolabelling. For fibronectin and Ki67 staining samples
359 are permeabilized with Triton X 0.5% in TBS (Sigma T8787) for 15 minutes at RT. Nonspecific sites
360 are blocked with 3% BSA (Bovine serum Albumin) for 1 hour. Then, samples are incubated with
361 first antibody (Fibronectin, Sigma F7387, 1/200 and Ki67; Millipore ab9260, 1/500) overnight at 4°C.
362 Subsequently samples are thoroughly washed with TBS three times, for 15 minutes each. A second
363 fluorescent antibody (goat anti-mouse Cy3, Invitrogen; 1/1000) is incubated for 40 minutes along
364 with phalloidin (1/500, Alexa Fluor 488, Thermo Fisher Scientific). After extensive washing with
365 TBS (four washes of 15 minutes) glass cover slides are mounted on the glass slides with a Proglod
366 mounting medium overnight (Life Technologies P36965) and stored at 4°C before imaging.

367 **5.8 Statistical analysis**

368 Student's t-test (unpaired, two tailed, equal variances) is used to calculate statistical significance
369 as appropriate by using PRISM version 7 (graphpad Software). Statistical significance is given by *,
370 P<0.05; **, P<0.01; ***, P<0.001; ****, P<0.0001.

371 **References**

- 372 Alessandri, K., Sarangi, B. R., Gurchenkov, V. V., Sinha, B., Kiessling, T. R., Fetler, L., Rico, F., Scheuring, S., Lamaze,
373 C., Simon, A., Geraldo, S., Vignjevic, D., Domejean, H., Rolland, L., Funfak, A., Bibette, J., Bremond, N., and
374 Nassoy, P. (2013). Cellular capsules as a tool for multicellular spheroid production and for investigating the
375 mechanics of tumor progression in vitro. *Proceedings of the National Academy of Sciences*, 110(37):14843-
376 14848.
- 377 Baranowski, B. (1991). Non-equilibrium thermodynamics as applied to membrane transport. *Journal of mem-*
378 *brane science*, 57(2):119-159.

- 379 Barrat, J.-L. and Joanny, J.-F. (1997). Theory of polyelectrolyte solutions. *Advances in Chemical Physics, Polymeric*
380 *Systems*, page 1.
- 381 Barriga, E. H., Franze, K., Charras, G., and Mayor, R. (2018). Tissue stiffening coordinates morphogenesis by
382 triggering collective cell migration in vivo. *Nature*, 554(7693):523–527.
- 383 Bastide, J., Candau, S., and Leibler, L. (1981). Osmotic deswelling of gels by polymer solutions. *Macromolecules*,
384 14(3):719–726.
- 385 Bissell, M. J., Radisky, D. C., Rizki, A., Weaver, V. M., and Petersen, O. W. (2002). The organizing principle: mi-
386 croenvironmental influences in the normal and malignant breast. *Differentiation*, 70(9-10):537–546.
- 387 Bläßle, A., Soh, G., Braun, T., Mörsdorf, D., Preiß, H., Jordan, B. M., and Müller, P. (2018). Quantitative diffusion
388 measurements using the open-source software pyfrap. *Nature communications*, 9(1):1–14.
- 389 Brochard, F. (1981). Polymer networks swollen by a homopolymer solution. *Journal de Physique*, 42(3):505–511.
- 390 Broders-Bondon, F., Nguyen Ho-Bouloires, T. H., Fernandez-Sanchez, M.-E., and Farge, E. (2018). Mechan-
391 otransduction in tumor progression: The dark side of the force. *The Journal of Cell Biology*, 217(5):1571–1587.
- 392 Brunel, B., Levy, V., Millet, A., Dolega, M. E., Delon, A., Pierrat, R., and Cappello, G. (2020). Measuring cell
393 displacements in opaque tissues: dynamic light scattering in the multiple scattering regime. *Biomedical*
394 *optics express*, 11(4):2277–2297.
- 395 Butcher, D. T., Alliston, T., and Weaver, V. M. (2009). A tense situation: Forcing tumour progression. *Nature*
396 *Reviews Cancer*, 9(2):108–22.
- 397 Cadart, C., Venkova, L., Recho, P., Lagomarsino, M. C., and Piel, M. (2019). The physics of cell-size regulation
398 across timescales. *Nature Physics*, 15(10):993–1004.
- 399 Cadart, C., Zlotek-Zlotkiewicz, E., Venkova, L., Thouvenin, O., Racine, V., Le Berre, M., Monnier, S., and Piel, M.
400 (2017). *Fluorescence eXclusion Measurement of volume in live cells*, volume 139. Elsevier Ltd.
- 401 Charras, G. T., Coughlin, M., Mitchison, T. J., and Mahadevan, L. (2008). Life and times of a cellular bleb. *Bio-*
402 *physical journal*, 94(5):1836–1853.
- 403 Choquet, D., Felsenfeld, D. P., and Sheetz, M. P. (1997). Extracellular matrix rigidity causes strengthening of
404 integrin- cytoskeleton linkages. *Cell*, 88(1):39–48.
- 405 Clark, A. G. and Paluch, E. (2011). Mechanics and regulation of cell shape during the cell cycle. In *Cell cycle in*
406 *development*, pages 31–73. Springer.
- 407 Day, R. E., Kitchen, P., Owen, D. S., Bland, C., Marshall, L., Conner, A. C., Bill, R. M., and Conner, M. T. (2014). Hu-
408 man aquaporins: regulators of transcellular water flow. *Biochimica et Biophysica Acta (BBA)-General Subjects*,
409 1840(5):1492–1506.
- 410 Delarue, M., Montel, F., Vignjevic, D., Prost, J., Joanny, J. F. J.-F., and Cappello, G. (2014). Compressive stress
411 inhibits proliferation in tumor spheroids through a volume limitation. *Biophysical Journal*, 107(8):1821–1828.
- 412 Diz-Muñoz, A., Krieg, M., Bergert, M., Ibarlucea-Benitez, I., Muller, D. J., Paluch, E., and Heisenberg, C.-P. (2010).
413 Control of directed cell migration in vivo by membrane-to-cortex attachment. *PLoS biology*, 8(11):e1000544.
- 414 Dolega, M. E., Delarue, M., Ingremeau, F., Prost, J., Delon, A., and Cappello, G. (2017). Cell-like pressure sensors
415 reveal increase of mechanical stress towards the core of multicellular spheroids under compression. *Nature*
416 *Communications*, 8(May 2016):1–9.
- 417 Elmoazzen, H. Y., Elliott, J. A., and McGann, L. E. (2009). Osmotic transport across cell membranes in nondilute
418 solutions: a new nondilute solute transport equation. *Biophysical Journal*, 96(7):2559–2571.
- 419 Engler, A. J., Sen, S., Sweeney, H. L., and Discher, D. E. (2006). Matrix Elasticity Directs Stem Cell Lineage Specifi-
420 cation. *Cell*, 126(4):677–689.
- 421 Fernandez-Sanchez, M.-E., Serman, F., Ahmadi, P., and Farge, E. (2010). Mechanical induction in embryonic de-
422 velopment and tumor growth: integrative cues through molecular to multicellular interplay and evolutionary
423 perspectives. In *Methods in cell biology*, volume 98, pages 295–321. Elsevier.
- 424 Granath, K. A. (1958). Solution properties of branched dextrans. *Journal of Colloid Science*, 13(4):308–328.

- 425 Guo, M., Pegoraro, A. F., Mao, A., Zhou, E. H., Arany, P. R., Han, Y., Burnette, D. T., Jensen, M. H., Kasza, K. E.,
426 Moore, J. R., Mackintosh, F. C., Fredberg, J. J., Mooney, D. J., Lippincott-Schwartz, J., and Weitz, D. A. (2017).
427 Cell volume change through water efflux impacts cell stiffness and stem cell fate. *Proceedings of the National*
428 *Academy of Sciences of the United States of America*, 114(41):E8618–E8627.
- 429 Han, Y. L., Pegoraro, A. F., Li, H., Li, K., Yuan, Y., Xu, G., Gu, Z., Sun, J., Hao, Y., Gupta, S. K., Li, Y., Tang, W., Kang,
430 H., Teng, L., Fredberg, J. J., and Guo, M. (2020). Cell swelling, softening and invasion in a three-dimensional
431 breast cancer model. *Nature Physics*, 16(1):101–108.
- 432 Hawkins, R. J., Poincloux, R., Bénichou, O., Piel, M., Chavrier, P., and Voituriez, R. (2011). Spontaneous
433 contractility-mediated cortical flow generates cell migration in three-dimensional environments. *Biophysic-*
434 *cal journal*, 101(5):1041–1045.
- 435 Helmlinger, G., Netti, P. A., Lichtenbeld, H. C., Melder, R. J., and Jain, R. K. (1997). Solid stress inhibits the growth
436 of multicellular tumor spheroids. *Nature biotechnology*, 15:778–783.
- 437 Hodgkin, A. and Huxley, A. (1952). Propagation of electrical signals along giant nerve fibres. *Proceedings of the*
438 *Royal Society of London. Series B, Biological Sciences*, pages 177–183.
- 439 Hoffmann, E. K., Lambert, I. H., and Pedersen, S. F. (2009). Physiology of cell volume regulation in vertebrates.
440 *Physiological reviews*, 89(1):193–277.
- 441 Hoppensteadt, F. C. and Peskin, C. S. (2012). *Modeling and simulation in medicine and the life sciences*, volume 10.
442 Springer Science & Business Media.
- 443 Hui, T., Zhou, Z., Qian, J., Lin, Y., Ngan, A., and Gao, H. (2014). Volumetric deformation of live cells induced by
444 pressure-activated cross-membrane ion transport. *Physical review letters*, 113(11):118101.
- 445 Humphrey, J. D., Dufresne, E. R., and Schwartz, M. A. (2014). Mechanotransduction and extracellular matrix
446 homeostasis. *Nature Reviews Molecular Cell Biology*, 15(12):802–812.
- 447 Isenberg, B. C., DiMilla, P. A., Walker, M., Kim, S., and Wong, J. Y. (2009). Vascular smooth muscle cell durotaxis
448 depends on substrate stiffness gradient strength. *Biophysical Journal*, 97(5):1313–1322.
- 449 Julicher, F., Kruse, K., Prost, J., and Joanny, J.-F. (2007). Active behavior of the cytoskeleton. *Physics reports*,
450 449(1-3):3–28.
- 451 Kedem, O. and Katchalsky, A. (1963). Permeability of composite membranes. part 1. electric current, volume
452 flow and flow of solute through membranes. *Trans. Faraday Soc.*, 59:1918–1930.
- 453 Kedem, O. t. and Katchalsky, A. (1958). Thermodynamic analysis of the permeability of biological membranes
454 to non-electrolytes. *Biochimica et biophysica Acta*, 27:229–246.
- 455 Kim, D.-H., Li, B., Si, F., Phillip, J. M., Wirtz, D., and Sun, S. X. (2015). Volume regulation and shape bifurcation in
456 the cell nucleus. *Journal of cell science*, 128(18):3375–3385.
- 457 Kleinman, H. K. and Martin, G. R. (2005). Matrigel: basement membrane matrix with biological activity. In
458 *Seminars in cancer biology*, volume 15, pages 378–386. Elsevier.
- 459 Kurniawan, N. A., Chaudhuri, P. K., and Lim, C. T. (2016). Mechanobiology of cell migration in the context of
460 dynamic two-way cell-matrix interactions. *Journal of Biomechanics*, 49(8):1355–1368.
- 461 Lang, F., Busch, G. L., Ritter, M., VÖLKL, H., Waldegger, S., Gulbins, E., and HÄUSSINGER, D. (1998). Functional
462 significance of cell volume regulatory mechanisms. *Physiological reviews*, 78(1):247–306.
- 463 Lelièvre, S. A. and Bissell, M. J. (2006). Three dimensional cell culture: the importance of microenvironment in
464 regulation of function. *Reviews in Cell Biology and Molecular Medicine*.
- 465 Levental, K. R., Yu, H., Kass, L., Lakins, J. N., Egeblad, M., Erler, J. T., Fong, S. F., Csiszar, K., Giaccia, A., Weninger,
466 W., Yamauchi, M., Gasser, D. L., and Weaver, V. M. (2009). Matrix Crosslinking Forces Tumor Progression by
467 Enhancing Integrin Signaling. *Cell*, 139(5):891–906.
- 468 Luo, C.-h. and Rudy, Y. (1991). A model of the ventricular cardiac action potential. depolarization, repolarization,
469 and their interaction. *Circulation research*, 68(6):1501–1526.
- 470 Milo, R. (2013). What is the total number of protein molecules per cell volume? a call to rethink some published
471 values. *Bioessays*, 35(12):1050–1055.

- 472 Monnier, S., Delarue, M., Brunel, B., M., D., E., Delon, A., Cappello, G., Dolega, M. M. E., Delon, A., and Cappello,
473 G. (2015). Effect of an osmotic stress on multicellular aggregates. *Methods*, 94:114–119.
- 474 Montel, F., Delarue, M., Elgeti, J., Malaquin, L., Basan, M., Risler, T., Cabane, B., Vignjevic, D., Prost, J., Cappello, G.,
475 and Joanny, J.-F. (2011). Stress clamp experiments on multicellular tumor spheroids. *Physical Review Letters*,
476 107(18):1–4.
- 477 Mori, Y. (2012). Mathematical properties of pump-leak models of cell volume control and electrolyte balance.
478 *Journal of mathematical biology*, 65(5):875–918.
- 479 Nam, S., Gupta, V. K., Lee, H.-p., Lee, J. Y., Wisdom, K. M., Varma, S., Flaum, E. M., Davis, C., West, R. B., and Chaud-
480 huri, O. (2019). Cell cycle progression in confining microenvironments is regulated by a growth-responsive
481 TRPV4-PI3K/Akt-p27 ^{^{Kip1} signaling axis. *Science Advances*, 5(8):eaaw6171.}
- 482 Nia, H. T., Liu, H., Seano, G., Datta, M., Jones, D., and Rahbari, N. (2016). Solid stress and elastic energy as
483 measures of tumour mechanopathology. *Nature Publishing Group*, 1(November):1–11.
- 484 Panzetta, V., Fusco, S., and Netti, P. A. (2019). Cell mechanosensing is regulated by substrate strain energy
485 rather than stiffness. *Proceedings of the National Academy of Sciences*, 116(44):22004–22013.
- 486 Paszek, M. J., Zahir, N., Johnson, K. R., Lakins, J. N., Rozenberg, G. I., Gefen, A., Reinhart-King, C. A., Margulies,
487 S. S., Dembo, M., Boettiger, D., Hammer, D. A., and Weaver, V. M. (2005). Tensional homeostasis and the
488 malignant phenotype. *Cancer Cell*, 8(3):241–254.
- 489 Pelham, R. J. and Wang, Y. L. (1997). Cell locomotion and focal adhesions are regulated by substrate flexibility.
490 *Proceedings of the National Academy of Sciences of the United States of America*, 94(25):13661–13665.
- 491 Roycroft, A. and Mayor, R. (2016). Molecular basis of contact inhibition of locomotion. *Cellular and Molecular
492 Life Sciences*, 73(6):1119–1130.
- 493 Salbreux, G., Charras, G., and Paluch, E. (2012). Actin cortex mechanics and cellular morphogenesis. *Trends in
494 cell biology*, 22(10):536–545.
- 495 Sedzinski, J., Biro, M., Oswald, A., Tinevez, J.-Y., Salbreux, G., and Paluch, E. (2011). Polar actomyosin contractility
496 destabilizes the position of the cytokinetic furrow. *Nature*, 476(7361):462–466.
- 497 Segel, M., Neumann, B., Hill, M. F. E., Weber, I. P., Viscomi, C., Zhao, C., Young, A., Agle, C. C., Thompson, A. J.,
498 Gonzalez, G. A., Sharma, A., Holmqvist, S., Rowitch, D. H., Franze, K., Franklin, R. J. M., and Chalut, K. J. (2019).
499 Niche stiffness underlies the ageing of central nervous system progenitor cells. *Nature*, 573(7772):130–134.
- 500 Sopher, R. S., Tokash, H., Natan, S., Sharabi, M., Shelah, O., Tchaicheeyan, O., and Lesman, A. (2018). Nonlinear
501 Elasticity of the ECM Fibers Facilitates Efficient Intercellular Communication. *Biophysical Journal*, 115(7):1357–
502 1370.
- 503 Staunton, J. R., So, W. Y., Paul, C. D., and Tanner, K. (2019). High-frequency microrheology in 3D reveals mis-
504 match between cytoskeletal and extracellular matrix mechanics. *Proceedings of the National Academy of Sci-
505 ences*, 116(29):14448–14455.
- 506 Staverman, A. (1952). Non equilibrium thermodynamics of membrane processes. *Trans. Faraday Soc.*, 48:176–
507 185.
- 508 Strange, K. (1993). *Cellular and molecular physiology of cell volume regulation*. CRC Press.
- 509 Sunyer, R., Conte, V., Escribano, J., Elosegui-Artola, A., Labernadie, A., Valon, L., Navajas, D., García-Aznar, J. M.,
510 Muñoz, J. J., Roca-Cusachs, P., and Trepast, X. (2016). Collective cell durotaxis emerges from long-range inter-
511 cellular force transmission. *Science*, 353(6304):1157–1161.
- 512 Tanner, K., Mori, H., Mroue, R., Bruni-Cardoso, A., and Bissell, M. J. (2012). Coherent angular motion in the es-
513 tablishment of multicellular architecture of glandular tissues. *Proceedings of the National Academy of Sciences*,
514 109(6):1973–1978.
- 515 Taubenberger, A. V., Girardo, S., Träber, N., Fischer-Friedrich, E., Kräter, M., Wagner, K., Kurth, T., Richter, I.,
516 Haller, B., Binner, M., Hahn, D., Freudenberg, U., Werner, C., and Guck, J. (2019). Hydrogels: 3D Microenvi-
517 ronment Stiffness Regulates Tumor Spheroid Growth and Mechanics via p21 and ROCK (Adv. Biosys. 9/2019).
518 *Advanced Biosystems*, 3(9):1970092.

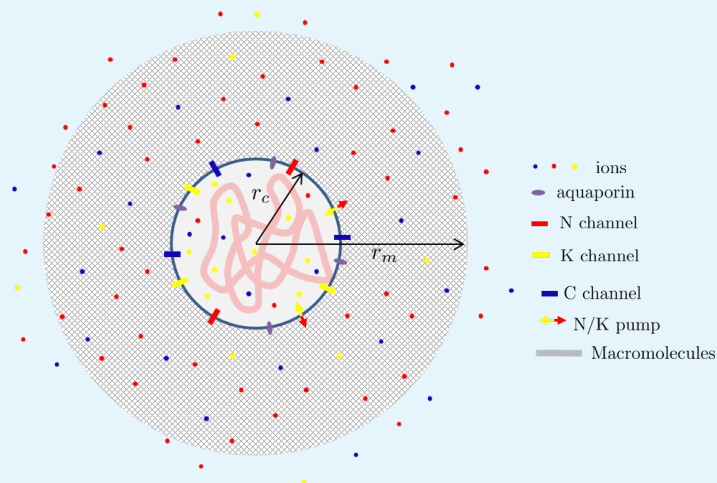
- 519 Therien, A. G. and Blostein, R. (2000). Mechanisms of sodium pump regulation. *American Journal of Physiology-*
520 *Cell Physiology*, 279(3):C541–C566.
- 521 Tinevez, J.-Y., Schulze, U., Salbreux, G., Roensch, J., Joanny, J.-F., and Paluch, E. (2009). Role of cortical tension in
522 bleb growth. *Proceedings of the National Academy of Sciences*, 106(44):18581–18586.
- 523 Turlier, H., Audoly, B., Prost, J., and Joanny, J.-F. (2014). Furrow constriction in animal cell cytokinesis. *Biophysical*
524 *journal*, 106(1):114–123.
- 525 Vogel, V. (2018). Unraveling the Mechanobiology of Extracellular Matrix. *Annual Review of Physiology*, 80(1):353–
526 387.
- 527 Voutouri, C., Polydorou, C., Papageorgis, P., Gkretsi, V., and Stylianopoulos, T. (2016). Hyaluronan-Derived
528 Swelling of Solid Tumors, the Contribution of Collagen and Cancer Cells, and Implications for Cancer Therapy.
529 *Neoplasia (United States)*, 18(12):732–741.
- 530 Yi, C.-S., Fogelson, A. L., Keener, J. P., and Peskin, C. S. (2003). A mathematical study of volume shifts and ionic
531 concentration changes during ischemia and hypoxia. *Journal of Theoretical Biology*, 220(1):83–106.
- 532 Zhou, E., Trepats, X., Park, C., Lenormand, G., Oliver, M., Mijailovich, S., Hardin, C., Weitz, D., Butler, J., and
533 Fredberg, J. (2009). Universal behavior of the osmotically compressed cell and its analogy to the colloidal
534 glass transition. *Proceedings of the National Academy of Sciences*, 106(26):10632–10637.
- 535 Zlotek-Zlotkiewicz, E., Monnier, S., Cappello, G., Le Berre, M., and Piel, M. (2015). Optical volume and mass
536 measurements show that mammalian cells swell during mitosis. *Journal of Cell Biology*, 211(4):765–774.

537 **Appendix 1**538 **A Theoretical model of the osmotic compression of a single cell nested**
539 **in matrigel**

540 Our aim is to qualitatively understand the nature of the steady state mechanical stress and
541 displacement of a cell nested in a matrix in two paradigmatic situations:

- 542 • when some small osmolites (typically dextran) that can permeate the matrix pores are
543 introduced in the solution,
- 544 • when some big osmolites that are excluded from the matrix are introduced in the
545 solution.

546 The matrix is a meshwork of biopolymers permeated by an aqueous solution containing
547 ions. These ions can also permeate the cell cytoplasm via specific channels and pumps inte-
548 grated in the plasmic membrane (*Hoffmann et al., 2009; Lang et al., 1998*). For simplicity, we
549 restrict our theoretical description to Na^+ , K^+ and Cl^- ions which have specific channels and
550 a well studied pump (*Therien and Blostein, 2000*) which actively pumps out three sodium
551 ions in exchange of having two potassium ions in. Attached right under the cell membrane
552 via some specific cross-linkers (*Diz-Muñoz et al., 2010*), the cell cortex is a thin 'muscle-like'
553 actin network cross-linked by passive and contractile cross-linkers such as myosin II. The
554 cortex has been shown to be an important regulator of the cell surface tension (*Clark and*
555 *Paluch, 2011; Salbreux et al., 2012*) as exemplified during motility (*Hawkins et al., 2011*) and
556 cell morphogenesis (*Turlier et al., 2014; Sedzinski et al., 2011; Tinevez et al., 2009; Charras*
557 *et al., 2008*). The cell membrane and cortex enclose the cytoplasm a meshwork of macro-
558 molecules permeated by water and containing the aforementioned ions. See Fig. 1 for a
559 scheme of the model.



560 **Appendix 1 Figure 1.** Scheme of a cell nested in a porous matrix.

563 For simplicity we assume a spherical geometry with a cell of radius r_c inside a matrix
564 ball of radius r_m . Each point in the space \mathbf{x} can therefore be localized by its radial position
565 $\mathbf{x} = r\mathbf{e}_r$ where \mathbf{e}_r is radial unit vector. We assume a spherical symmetry of the problem such
566 that all the introduced physical fields are independent of the angular coordinates θ and φ .
567 Throughout this text, we restrict ourselves to a linear theory which typically holds when the
568 deformation in the matrix is assumed to remain sufficiently small.

569 **A.1 Conservation laws at the cell-matrix interface**

571
572
573
574
575
576
577
578
579
580
581
582
583
584
585
586
587
588
589
590
591
592
593
594
595
596
597
598
599
600
601
602
603
604
605
606
607
608
609
610
611
612
613

Water conservation.

From Kedem-Katchalsky theory (*Staverman, 1952; Kedem and Katchalsky, 1958, 1963; Baranowski, 1991; Elmoazzen et al., 2009*), assuming that the aqueous solvent moves through specific and passive channels, the aquaporins (*Day et al., 2014*), we can express the incoming water flux \mathbf{j}_w at $r = r_c$ as (*Yi et al., 2003; Hui et al., 2014; Strange, 1993; Hoffmann et al., 2009; Mori, 2012; Cadart et al., 2019*):

$$\mathbf{j}_w \cdot \mathbf{e}_r = L_p [p_m - p_c - (\Pi_m - \Pi_c)], \quad (4)$$

where $\Pi_{m,c}$ denote the osmotic pressures in the matrix phase and the cell while $p_{m,c}$ are the hydrostatic pressures defined with respect to the external (i.e. atmospheric) pressure. The so-called filtration coefficient L_p is related to the permeability of aquaporins. In a dilute approximation which we again assume for simplicity, the osmotic pressure is dominated by the small molecules in solution and thus reads

$$\Pi_m = k_B T (N_m + K_m + C_m + D_m) \text{ and} \quad \Pi_c = k_B T (N_c + K_c + C_c), \quad (5)$$

where k_B is the Boltzmann constant, T the temperature, $N_{c,m}$, $K_{c,m}$ and $C_{c,m}$ are the (number) concentrations of sodium, potassium and chloride in the cytoplasm and the extra-cellular medium and D_m is the extra-cellular Dextran (necessary small as big are excluded) concentration in the matrix phase. We neglect in (5) the osmotic contribution associated with the large macromolecules composing the cell organelles and the cytoskeleton compared to the ionic contributions. In a similar manner, the osmotic contribution of the matrix polymer is also neglected. At steady state, the water flux vanishes ($\mathbf{j}_w = 0$) leading to the relation at $r = r_c$,

$$p_m - p_c = \Pi_m - \Pi_c. \quad (6)$$

Ions conservation.

As each ion travels through the plasma membrane via specific channels and pumps, the intensities of each ionic current at $r = r_c$ is given by Nernst-Planck laws (*Mori, 2012*),

$$\begin{aligned} i_N &= g_N \left[v_c - \frac{k_B T}{q} \log \left(\frac{N_m}{N_c} \right) \right] + 3qj_p \\ i_K &= g_K \left[v_c - \frac{k_B T}{q} \log \left(\frac{K_m}{K_c} \right) \right] - 2qj_p \\ i_C &= g_C \left[v_c + \frac{k_B T}{q} \log \left(\frac{C_m}{C_c} \right) \right], \end{aligned} \quad (7)$$

where $g_{N,K,C}$ are the respective conductivities of ions, v_c is the cell membrane potential, q is the elementary charge and j_p is the pumping rate associated to the Na-K pump on the membrane which is playing a fundamental role for cellular volume control (*Hoffmann et al., 2009*). The factors 3 and 2 are related to the stoichiometry of the sodium potassium pump. Again, in steady state, currents $i_{N,K,C} = 0$, leading to the Gibbs-Donnan equilibrium:

$$N_c = N_m e^{-\frac{q(v_c - v_N)}{k_B T}}, \quad K_c = K_m e^{-\frac{q(v_c - v_K)}{k_B T}} \text{ and} \quad C_c = C_m e^{\frac{qv_c}{k_B T}}, \quad (8)$$

where the active potentials related to the pumping activity $v_{N,K}$ are $v_N = -3qj_p/g_N$ and $v_K = 2qj_p/g_K$.

614

615

616

617

618

619

620

621

622

623

624

625

626

627

628

629

630

631

632

633

634

635

636

637

638

639

640

641

642

643

644

645

646

647

648

649

650

651

652

653

654

655

656

657

Supposing that the cell membrane capacitance is vanishingly small (*Mori, 2012*), we can neglect the presence of surface charges and impose an electro-neutrality constraint for the intra-cellular medium:

$$N_c - C_c + K_c - \rho_c z_c = 0, \quad (9)$$

where z_c is the average number of (negative in the physiological pH = 7.4 conditions) electric charges carried by macromolecules inside the cell and ρ_c is their density. As macromolecules are trapped inside the cell membrane, we can express $\rho_c = X_c/(4\pi r_c^3/3)$ where X_c is the number of macro-molecules which is fixed at short timescale and only increases slowly through synthesis as the amount of dry mass doubles during the cell cycle.

Force balance.

At the interface between the cell and the matrix ($r = r_c$), we can express the mechanical balance as

$$\Sigma_c^{\text{bulk}} \mathbf{e}_r + \sigma_c^{\text{surf}} \mathbf{e}_r = \Sigma_m \mathbf{e}_r. \quad (10)$$

In (10), Σ_c^{bulk} is the Cauchy stress in the cytoplasm which we decompose into $\Sigma_c^{\text{bulk}} = \Sigma_c^{\text{skel}} - p_c \mathbf{I}$, with a first contribution due to the cytoskeleton and a second contribution due to the hydrostatic pressure in the cytosol. The identity matrix is denoted \mathbf{I} . The contribution due to the mechanical resistance of the cortex and membrane is denoted σ_c^{surf} . In our spherical geometry, we can express $\sigma_c^{\text{surf}} = 2\gamma_c/r_c$ where γ_c is a surface tension in the cell contour. Finally Σ_m is the stress in the matrix phase for which we postulate a poro-elastic behavior such that, $\Sigma_m = \Sigma_m^{\text{el}}(\epsilon_m) - p_m \mathbf{I}$ where

$$\Sigma_m^{\text{el}} = 2G\mathbf{E}_m + \left(K_d - \frac{2G}{3}\right) \text{tr}(\mathbf{E}_m)\mathbf{I}, \quad (11)$$

is the Hooke's law with \mathbf{E}_m the (small) elastic strain in the matrix, G the shear modulus and K_d the drained bulk modulus.

In the absence of cytoskeleton and external matrix, (10) reduces to Laplace law:

$$\frac{2\gamma_c}{r_c} = p_c - p_m$$

and more generally reads,

$$(\Sigma_c^{\text{skel}} - \Sigma_m^{\text{el}})\mathbf{e}_r \cdot \mathbf{e}_r + \frac{2\gamma_c}{r_c} = p_c - p_m. \quad (12)$$

Such relation provides the hydrostatic pressure jump at the cell membrane ($r = r_c$) entering in the osmotic balance (6) and, combining (6) and (12), we obtain

$$(\Sigma_c^{\text{skel}} - \Sigma_m^{\text{el}})\mathbf{e}_r \cdot \mathbf{e}_r + \frac{2\gamma_c}{r_c} = \Pi_c - \Pi_m. \quad (13)$$

A.2 Conservation laws in the extra-cellular matrix

Water conservation.

Assuming that the extra-cellular fluid follows a Darcy law, mass conservation of the incompressible water permeating the matrix can be expressed as

$$\partial_t n - \frac{\kappa}{\mu} \frac{1}{r} \frac{d}{dr} \left(r \frac{dp_m}{dr} \right) = 0, \quad (14)$$

where n is the matrix porosity, κ the matrix permeability and μ the fluid viscosity. In steady state, $\partial_t n = 0$ and (14) is associated with no flux boundary conditions at r_c and r_m given by

$$\frac{dp_m}{dr} \Big|_{r_m, r_c} = 0.$$

It follows that p_m is homogeneous in the matrix and its value is imposed by a relation similar to (6) with an infinitely permeable membrane at r_m :

$$p_m(r) = \Pi_m - \Pi_e. \quad (15)$$

In (15), Π_e is the external osmotic pressure which reads

$$\Pi_e = k_B T (N_e + K_e + C_e + D_e) \quad (16)$$

where N_e , K_e and C_e denote the ions concentrations in the external solution and D_e the concentration of Dextran added to the external solution.

Ions conservation.

As we are interested about the steady-state only, the Poisson-Nernst fluxes of ions concentrations in the matrix locally vanish leading to:

$$\frac{dN_m}{dr} + \frac{N_m q}{k_B T} \frac{dv_m}{dr} = \frac{dK_m}{dr} + \frac{K_m q}{k_B T} \frac{dv_m}{dr} = \frac{dC_m}{dr} - \frac{C_m q}{k_B T} \frac{dv_m}{dr} = 0,$$

where $v_m(r)$ is the electro-static potential in the matrix.

As v_m is defined up to an additive constant, we chose that $v_m(r_m) = 0$ and, imposing the continuity of ions concentrations at the transition between the matrix and the external solution $N_m|_{r_m} = N_e$, $K_m|_{r_m} = K_e$ and $C_m|_{r_m} = C_e$, we obtain

$$N_m = N_e e^{-\frac{qv_m}{k_B T}}, \quad K_m = K_e e^{-\frac{qv_m}{k_B T}} \quad \text{and} \quad C_m = C_e e^{\frac{qv_m}{k_B T}}. \quad (17)$$

Next, we again suppose for simplicity that the capacitance of both the porous matrix and the external media are vanishingly small leading to the electro-neutrality constraints

$$\begin{aligned} N_m + K_m - C_m - z_m \rho_m &= 0 \\ N_e + K_e - C_e &= 0, \end{aligned} \quad (18)$$

where z_m is the number of negative charges carried by the biopolymer chains forming the matrix and ρ_m is their density. As we use uncharged Dextran, its concentration does not enter in expressions (18). Using, (17) in tandem with (18), we obtain

$$v_m = -\frac{k_B T}{q} \sinh^{-1} \left(\frac{z_m \rho_m}{2C_e} \right). \quad (19)$$

Re-injecting this expression into (17), we obtain the steady state concentrations of ions in the matrix phase:

$$\begin{aligned} N_m &= N_e e^{\sinh^{-1} \left(\frac{z_m \rho_m}{2C_e} \right)}, \quad K_m = K_e e^{\sinh^{-1} \left(\frac{z_m \rho_m}{2C_e} \right)} \\ \text{and } C_m &= C_e e^{-\sinh^{-1} \left(\frac{z_m \rho_m}{2C_e} \right)}. \end{aligned} \quad (20)$$

Next, we make the realistic assumption that the chloride concentration (number of ions per unit volume) is much larger than the density of fixed charges carried by the polymer chains (number charges per unit volume): $z_m \rho_m / C_e \ll 1$. Indeed using the rough estimates of Section A.4, the average number of charge carried per amino-acid is 0.06 and the typical concentration of matrix is 5 g/L. As the molar mass of an amino-acid is roughly 150g/mol,

we obtain that $z_m \rho_m \simeq 2\text{mM}$ while $C_e \simeq 100\text{mM}$. We can thus simplify (20) up to first order to obtain,

$$N_m = N_e \left(1 + \frac{z_m \rho_m}{2C_e} \right), K_m = K_e \left(1 + \frac{z_m \rho_m}{2C_e} \right) \text{ and} \quad C_m = C_e \left(1 - \frac{z_m \rho_m}{2C_e} \right). \quad (21)$$

As a result, we obtain that the only steady state contribution of

$$\begin{aligned} \Pi &\stackrel{\text{def}}{=} \Pi_e - \Pi_m = k_B T (D_e - D_m) \\ &= \begin{cases} 0 & \text{for small Dextran} \\ k_B T D_e & \text{for big Dextran,} \end{cases} \end{aligned} \quad (22)$$

is imposed by Dextran since the ions only start to contribute to this difference at second order in the small parameter $z_m \rho_m / C_e$. We therefore conclude that, in good approximation, Π vanishes for small Dextran molecules that can permeate the matrix and equates to the imposed and known quantity $k_B T D_e$ for big Dextran molecules that cannot enter the matrix pores.

It then follows from (15) that the hydrostatic pressure equilibrates with the imposed osmotic pressure,

$$p_m(r) = -\Pi. \quad (23)$$

Force balance.

Using the spherical symmetry of the problem, the only non vanishing components of the stress tensor are Σ_m^{rr} and $\Sigma_m^{\theta\theta} = \Sigma_m^{\varphi\varphi}$. Therefore, the local stress balance reads

$$\frac{d\Sigma_m^{rr}}{dr} + \frac{2}{r}(\Sigma_m^{rr} - \Sigma_m^{\theta\theta}) = 0,$$

Assuming a small enough displacement, the non-vanishing components of the strain tensor are given by, $\mathbf{E}_m^{rr} = du_r/dr$ and $\mathbf{E}_m^{\theta\theta} = \mathbf{E}_m^{\varphi\varphi} = u_r/r$ where u_r is the radial (and only non-vanishing) displacement component from an homogeneous reference configuration corresponding to a situation where the matrix is not subjected to any external loading and $r_{c,m} = R_{c,m}$. Using the poro-elastic constitutive behavior (11), u_r satisfies

$$\left(K_d + \frac{4}{3}G \right) \left(\frac{d^2 u_r}{dr^2} + \frac{2}{r} \frac{du_r}{dr} - \frac{2}{r^2} u_r \right) = \frac{dp_m}{dr}. \quad (24)$$

This equation is supplemented with the traction free boundary condition at $r = r_m$

$$\Sigma_m \mathbf{e}_r = 0. \quad (25)$$

Combined with (23), the two above equations (24) and (25) lead to the solution

$$u_r(r) = \epsilon^0 r + \frac{r_m^3 (\Pi + 3K_d \epsilon^0)}{4Gr^2}, \quad (26)$$

where the introduced constants ϵ^0 is found using the displacement continuity at the cell matrix- interface:

$$u_r(r_c) = u \stackrel{\text{def}}{=} r_c - R_c, \quad (27)$$

with u given by the change of the cell radius from a reference configuration with radius R_c . The general expression of u_r therefore reads,

$$u_r(r) = \frac{ur_c^2 (4Gr^3 + 3K_d r_m^3) + \Pi r_m^3 (r_c^3 - r^3)}{r^2 (4Gr^3 + 3K_d r_m^3)}, \quad (28)$$

leading to the following form of the total mechanical stress in the surrounding matrix:

$$\Sigma_m(r) = \frac{2Gr_c^2(3K_d u + r_c \Pi)}{r^3 (4Gr_c^3 + 3K_d r_m^3)} \times \begin{pmatrix} 2(r^3 - r_m^3) & 0 & 0 \\ 0 & (2r^3 + r_m^3) & 0 \\ 0 & 0 & (2r^3 + r_m^3) \end{pmatrix}. \quad (29)$$

A.3 Formulation of the model

Combining (5) with (13) and taking into account (21), we obtain the relation linking the cell mechanics and the osmotic pressures inside the cell and outside the matrix:

$$(\Sigma_c^{\text{skel}} - \Sigma_m^{\text{el}}) \mathbf{e}_r \cdot \mathbf{e}_r + \frac{2\gamma_c}{r_c} = k_B T (N_c + K_c + C_c - N_e - K_e - C_e - D_m).$$

We suppose that the stress in the cytoskeleton is regulated at an homeostatic tension such that $\Sigma_c^{\text{skel}} \mathbf{e}_r \cdot \mathbf{e}_r \stackrel{\text{def}}{=} \Sigma_a$ is a fixed given constant modeling the spontaneous cell contractility. We can then linearize the cell mechanical contributions close to $r_c = R_c$ to obtain

$$\Sigma_c^{\text{skel}} \mathbf{e}_r \cdot \mathbf{e}_r + \frac{2\gamma_c}{r_c} = \tilde{\Sigma}_a - k_c u,$$

where $\tilde{\Sigma}_a = \Sigma_a + 2\gamma_c/R_c$ and the effective cell mechanical stiffness is $k_c = 2\gamma_c/R_c^2$.

Using and (23) and (29) close to $r_{c,m} = R_{c,m}$ we can express,

$$-\Sigma_m^{\text{el}} \mathbf{e}_r \cdot \mathbf{e}_r = \frac{12GK_d(R_m^3 - R_c^3)u + (4G + 3K_d)R_m^3 R_c \Pi}{4GR_c^4 + 3K_d R_c R_m^3}.$$

We therefore finally get the linear relation,

$$\tilde{\Sigma}_a + \tilde{k}u + \tilde{\alpha}\Pi = k_B T (N_c + K_c + C_c - N_e - K_e - C_e - D_m), \quad (30)$$

where,

$$\tilde{k} = -k_c + \frac{12GK_d(R_m^3 - R_c^3)}{4GR_c^4 + 3K_d R_c R_m^3} \text{ and } \tilde{\alpha} = \frac{(4G + 3K_d)R_m^3}{4GR_c^3 + 3K_d R_m^3}.$$

In the limit where $R_m \gg R_c$,

$$\tilde{k} = -k_c + \frac{4G}{3R_c} \text{ and } \tilde{\alpha} = 1 + \frac{4G}{3K_d}.$$

Next, using (8) and (21) and neglecting $z_m \rho_m / C_e \ll 1$ we obtain the relation linking the externally controlled osmolarity with the cell and matrix mechanics:

$$\frac{\tilde{\Sigma}_a + \tilde{k}u + (\tilde{\alpha} - 1)\Pi}{k_B T} = N_e \left(e^{-\frac{q(v-v_N)}{k_B T}} - 1 \right) + K_e \left(e^{-\frac{q(v-v_K)}{k_B T}} - 1 \right) + C_e \left(e^{\frac{qv}{k_B T}} - 1 \right) - D_e. \quad (31)$$

In a similar way, we combine (8) with (9) with again (21) in the limit where $z_m \rho_m / C_e \ll 1$ to express the electro-neutrality condition

$$N_e e^{-\frac{q(v-v_N)}{k_B T}} + K_e e^{-\frac{q(v-v_K)}{k_B T}} - C_e e^{\frac{qv}{k_B T}} = \frac{3z_c X_c}{4\pi R_c^3} \left(1 - \frac{3u}{R_c}\right), \quad (32)$$

where we have additionally linearized the right handside close to $r_c = R_c$.

The two equations (31) and (32) constitute our final model.

A.4 Cell volume in the reference situation

We begin by computing the cell radius and the cell membrane potential in the reference configuration where by definition $u = 0$ and $\Pi = D_e = 0$ as no Dextran is present at all. In this case, we solve for the membrane potential $v_c \stackrel{\text{def}}{=} V_c$ and radius R_c in (31) and (32) to find their reference values. This computation strictly follows (*Hoppensteadt and Peskin, 2012*).

Defining the non-dimensional parameters,

$$\beta = \frac{N_e e^{qv_N/(k_B T)} + K_e e^{qv_K/(k_B T)}}{C_e} \quad \text{and} \quad \sigma = \frac{\tilde{\Sigma}_a}{k_B T C_e}$$

we find the reference radius and membrane potential,

$$R_c = \left(\frac{3z_c X_c}{4\pi C_e \sqrt{(\sigma+2)^2 - 4\beta}} \right)^{1/3}$$

and

$$V_c = \frac{k_B T}{2q} \log \left(-\sqrt{(\sigma+2)^2 - 4\beta} + \sigma + 2 \right).$$

Given that the typical concentration of chloride ions outside the cell is of the order of 100 milimolar, the osmotic pressure $k_B T C_e$ is of the order 10^5 Pa (i.e. an atmosphere). In sharp contrast, the typical mechanical stresses in the cytoskeleton and the cortex are of the order of $10^2 - 10^3$ Pa (*Julicher et al., 2007*). Therefore the non-dimensional parameter σ is of the order of $\sigma \sim 10^{-3}$ and will be neglected in the following. We then finally obtain the reference values,

$$R_c = \left(\frac{3z_c X_c}{8\pi C_e \sqrt{1-\beta}} \right)^{1/3}, \quad V_c = \frac{k_B T}{q} \log \left(1 - \sqrt{1-\beta} \right).$$

The pumping rate enables the cell to maintain a finite a volume. When $j_p \rightarrow 0$, $\beta \rightarrow 1$ and the cell swells to infinity because nothing can balance the osmotic pressure due to the macromolecules trapped inside. So it is expected that dead cells will swell and lyse. The same happens if the pumping rate is too high. Indeed as the membrane permeability of potassium is higher than the one of sodium, if the pumping rate is very high, a lot of potassium ions will be brought in (more than sodium ions will be expelled out) and to equilibrate osmolarity with the exterior, water will come in until the cell bursts because of the potassium ions pumped inside. Between these two unphysiological situations, computing the variation of volume with respect to the pumping rate, one gets that this variation vanishes when,

$$j_p^{\text{opt}} = \frac{k_B T}{q^2} \frac{g_N g_K}{g_N + g_K} \log \left(\frac{N_e g_K}{K_e g_N} \right).$$

At such pumping rate the volume is less sensitive to small variations in the pumping rate that may occur.

849 Rough estimates.

850 The computation of the effective charge carried by macromolecules is complex. The folding
851 of proteins and the electrostatic screening of charges between them (Manning effect) plays
852 a role. See (*Barrat and Joanny, 1997*) for a review. We can still make a very rough estimate
853 in the following way. We assume that macromolecules are mostly proteins. At physiological
854 pH = 7.4, three types of amino-acids carry a positive charge, Lysine, Arginine, Histidine while
855 two others Aspartate and Glutamate carry a negative charge. Added to this, Histidine has a
856 pKa = 6 smaller than the pH so the ratio of [histidine neutral base]/[histidine charged acid]
857 is $10^{\text{pH}-\text{pKa}} = 25$. Hence the contribution of histidine may be neglected. The occurrence of
858 the aforementioned amino acids in the formation of proteins is also known. The average
859 length of proteins is roughly 400 amino acids. We subsequently obtain the average effective
860 number of negative charges as,
861

$$862 z_c = 400(9.9 + 10.8 - 7 - 5.3)/100 = 25.$$

863 Such estimate needs to be refined and account for sugars and other macromolecules which
864 carry more charges but a interval from $z_c = 10$ to $z_c = 100$ charges seems reasonable.

865 Estimate of β requires the knowledge of physiological external concentration of ions $C_e =$
866 150mM, $N_e = 140\text{mM}$ and $K_e = 10\text{mM}$ as well as conductances of sodium and potassium ions
867 through the plasmic membrane. Here again the situation is complicated since the dynamical
868 opening of channels due to some change in the membrane potential (*Hodgkin and Huxley,*
869 *1952*) as well as the mechanical opening mediated by membrane stretching can play a role
870 and affect these quantities. Nevertheless a rough estimate can be given (*Yi et al., 2003*)

$$871 g_N = 2 \times 10^{-6} \text{C.V}^{-1}.\text{s}^{-1} \text{ and } g_K = 4.5 \times 10^{-5} \text{C.V}^{-1}.\text{s}^{-1}$$

872 Also the pump rate is estimated in (*Luo and Rudy, 1991*),

$$873 j_p = 2.78 \times 10^{-12} \text{mol.s}^{-1}.$$

874 This pump rate is in good agreement with the optimal pump rate predicted by the model ,

$$875 j_p^{\text{opt}} = 3 \times 10^{-12} \text{mol.s}^{-1}.$$

876 This leads to an estimate of

$$877 \beta = 0.1.$$

878 The density of macromolecules inside the cell is then found to be $\rho_c = 3 \times 10^6$ macro-
879 molecules per μm^{-3} which is a correct order of magnitude (*Milo, 2013*). To further check the
880 soundness of the above theory we can also compute the membrane potential and obtain
881 $V_c = -73\text{mV}$ in good agreement with classical values .

882 A.5 Osmotic compression of the cell

883 We now consider the case where, from the reference configuration presented in the previ-
884 ous section we impose an additional osmotic pressure in the external solution with Dextran
885 polymers $\Pi_d = k_B T D_e$. We recall that according to formula (22), $\Pi = 0$ for small Dextran
886 molecules while $\Pi = \Pi_d$ for big Dextran molecules.

887 We use (31) and (32) to compute the ensuing small displacement u . Assuming in good
888 approximation that the osmotic pressure imposed by chloride ions is much larger (10^5 Pa)
889 than the mechanical resistance of the cell cortex and the external matrix (10^3 Pa) $k_B T C_e \gg$
890 $\tilde{k} R_c$ we find that,

$$891 u = - \frac{(z_c X_c)^{1/3} ((\tilde{\alpha} - 1)\Pi + \Pi_d)}{4 \cdot 3^{2/3} \pi^{1/3} (1 - \beta)^{7/6} C_e^{4/3} k_B T}.$$

Strikingly, making the realistic simplifying assumptions that $K_d \gg G$ and $R_m \gg R_c$, leads to the same displacement of the cell membrane in the two situations of small and big Dextran:

$$u = -\frac{D_e(z_c X_c)^{1/3}}{4 \cdot 3^{2/3} \pi^{1/3} (1 - \beta)^{7/6} C_e^{4/3}},$$

showing that the two different osmotic loading are not distinguishable at that level. The main text relation (1) is obtained by assuming that the osmotic pressure of negatively charged ions is half the osmotic pressure of all ions.

However, the mechanical stress applied of the cell is completely different in both situations. For small Dextran, the mechanical stress confining the cell reads,

$$T^{\text{small}} = \Sigma_m \mathbf{e}_r \cdot \mathbf{e}_r |_{R_c} = \frac{2D_e G}{3C_e(1 - \beta)}$$

while for big Dextran it reads,

$$T^{\text{big}} = \Sigma_m \mathbf{e}_r \cdot \mathbf{e}_r |_{R_c} = -\Pi_d + T^{\text{small}}.$$

Since $T^{\text{small}} \ll \Pi_d$ by at least one order of magnitude, the most important feature that changes between small and big Dextran is that $T^{\text{small}} > 0$ while $T^{\text{big}} < 0$. The physical picture behind this is that small Dextran compresses the cell without draining the water out of the matrix. Therefore, the cell behaves as a small inclusion which volume is reduced by the osmotic compression. In response, the matrix is elastically pulling back to balance the stress at the interface. In contrast, for big Dextran, the water is drained out of the matrix which therefore compresses the cell.

Another important aspect is that $|T^{\text{small}}/T^{\text{big}}| \ll 1$ so that the expansile stress applied on the cell through the matrix with small Dextran is negligible compared to the compressive stress applied on the cell by big Dextran. This is fully compatible with the idea that big Dextran induce a biological response of the cell while small Dextran is not even perceived by the cell.

Note that, like the membrane displacement, the variation of the membrane potential $v \stackrel{\text{def}}{=} v_c - V_c$ is the same in the two situations:

$$v = -\frac{k_B T}{q} \frac{D_e}{2\sqrt{1 - \beta} C_e},$$

where we have made the same previous simplifying assumptions that $k_B T C_e \gg \tilde{k} R_c$, $K_d \gg G$ and $R_m \gg R_c$. Again such variation is negligibly small in our conditions where $D_e \ll C_e$ by several order of magnitudes. This further indicates that the biological response of the cell in response to a big Dextran compression has a mechanical rather than an electro-static origin.